A Highly Phenotyped Open Access Repository of Alpha-1 Antitrypsin Deficiency Pluripotent Stem Cells

Joseph E. Kaserman,[1,2,5] Killian Hurley,[1,2,5] Mark Dodge,[1] Carlos Villacorta-Martin,[1] Marall Vedaie,[1] Jyh-Chang Jean,[1] Derek C. Liberti,[1] Marianne F. James,[1] Michelle I. Higgins,[1] Nora J. Lee,[1] George R. Washko,[3] Raul San Jose Estepar,[3] Jeffrey Teckman,[4] Darrell N. Kotton,[1,2] and Andrew A. Wilson[1,2,*]

[1]Center for Regenerative Medicine (CReM) of Boston University and Boston Medical Center, Boston, MA 02118, USA
[2]The Pulmonary Center and Department of Medicine, Boston University School of Medicine, Boston, MA 02118, USA
[3]Brigham and Women's Hospital, Boston, MA 02118, USA
[4]Saint Louis University, St Louis, MO 63104, USA
[5]Co-first author
*Correspondence: awilson@bu.edu
https://doi.org/10.1016/j.stemcr.2020.06.006

SUMMARY

Individuals with the genetic disorder alpha-1 antitrypsin deficiency (AATD) are at risk of developing lung and liver disease. Patient induced pluripotent stem cells (iPSCs) have been found to model features of AATD pathogenesis but only a handful of AATD patient iPSC lines have been published. To capture the significant phenotypic diversity of the patient population, we describe here the establishment and characterization of a curated repository of AATD iPSCs with associated disease-relevant clinical data. To highlight the utility of the repository, we selected a subset of iPSC lines for functional characterization. Selected lines were differentiated to generate both hepatic and lung cell lineages and analyzed by RNA sequencing. In addition, two iPSC lines were targeted using CRISPR/Cas9 editing to accomplish scarless repair. Repository iPSCs are available to investigators for studies of disease pathogenesis and therapeutic discovery.

INTRODUCTION

Alpha-1 antitrypsin deficiency (AATD) is a prominent cause of inherited lung and liver disease, affecting approximately 100,000 patients in the United States and accounts for an estimated 1%–4% of chronic obstructive pulmonary disease cases (American Thoracic Society and European Respiratory Society, 2003; Lieberman et al., 1986). Clinical disease results from mutations in the *SERPINA1* gene and associated dysfunction of alpha-1 antitrypsin (AAT) protein. While much has been learned about the mechanisms through which misfolded AAT proteins affect both the lung and the liver in the half century since the disease was first described (Eriksson, 1964; Laurell and Eriksson, 1963), significant gaps in our understanding of disease pathogenesis remain, underscoring an unmet need for models that faithfully recapitulate human disease mechanisms and capture AATD patient heterogeneity.

Patient-derived induced pluripotent stem cells (iPSCs) have emerged in recent years as a model system capable of reproducing human disease phenotypes, including AATD (Rashid et al., 2010; Segeritz et al., 2018; Tafaleng et al., 2015; Wilson et al., 2015). Through the application of directed differentiation protocols, these pluripotent cells can be utilized to study disease mechanisms in a variety of differentiated cell types, including those representing the two organs most affected in AATD, lung and liver (Jacob et al., 2017; McCauley et al., 2017; Rashid et al., 2010; Segeritz et al., 2018; Tafaleng et al., 2015; Wilson et al.,

2015). Patient iPSCs likewise allow the generation of multiple cell types from a single genetic background, a significant advantage in modeling multiorgan diseases (Leung et al., 2013).

However, despite the promise represented by this model for AATD studies, significant challenges must be overcome to fully realize their potential. For instance, only a small number of AATD patient iPSC lines have been published to date. Moreover, both institutional and legal barriers limit or prohibit sharing of some existing lines with academic and industry investigators thus preventing their use for further understanding disease mechanisms, for drug discovery, or for cell therapies. In addition, line-to-line variability in differentiation efficiency can limit the utility of specific lines to generate disease-relevant lineages and is not often reported. To address these challenges, we have developed a unique, large repository of iPSCs derived from comprehensively phenotyped AATD patients with associated participant consent that explicitly allows sharing and dissemination of both cells and associated clinical data. To further enhance the utility of this repository, we have systematically differentiated a subset of lines to lung and liver lineages to both quantify their differentiation capacity and analyze their transcriptome in comparison with primary controls. Here, we present this repository together with salient details of clinical lung and liver characterization to facilitate the application of constituent iPSC lines for advanced disease studies.
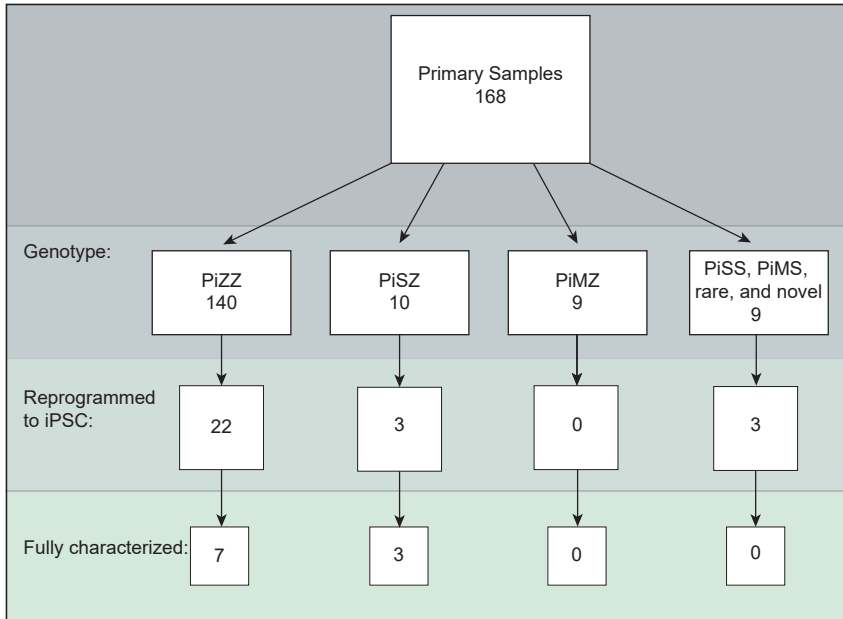
Figure 1. Flow Diagram of Individuals Included in Repository
See also Figures S1 and S2.

RESULTS

Establishment of an AATD iPSC Repository Representing Multiple Genotypes

To establish a freely accessible iPSC repository representing multiple AATD genotypes, we first compiled detailed clinical data, including radiographic and spirometric data, liver biochemistry and function testing, liver elastography, and biopsy results from patients attending the Alpha-1 Center at Boston University and Boston Medical Center and from subjects enrolled in two ongoing clinical studies. At the time of enrollment in the repository, we collected a linked sample of peripheral blood mononuclear cells (PBMCs) or in some cases skin fibroblasts suitable for reprogramming to generate iPSCs from each individual. We cryopreserved a total of 168 patient samples (Figure 1 and Table 1) representing both genders, a wide range of ages, and diverse *SERPINA1* genotypes, including common disease-causing variants (PiZZ, PiSZ), rare deficiency variants (PiQ0$_{Bolton}$Q0$_{Bolton}$, PiFZ, PiZM$_{Heerlen}$) (Reeves et al., 2018), and one newly described mutation (PiZV$_{Grantspass}$).

To provide a representative, diverse sampling of the repository, we next selected ten "featured" samples derived from individuals with PiZZ and PiSZ AAT phenotypes representing the most common pathogenic allele combinations for in-depth characterization of clinical phenotypic data as well as iPSC reprogramming and functional assays of resulting iPSCs following directed differentiation to disease-relevant lineages (Tables 2 and 3). Consistent with previous epidemiologic studies of AATD (American Thoracic Society and European Respiratory Society, 2003), the majority of the samples selected for characterization (8/10) are derived from individuals with radiographic (seven with emphysema, one with cystic lung disease) and spirometrically confirmed lung disease, while the remaining two samples represent younger subjects who have not to date developed detectable lung pathology (overall mean forced expiratory volume in 1 s [FEV1]/forced vital capacity [FVC] 49.4%; FEV1 58%; diffusion capacity for carbon monoxide in percent predicted 54.1%) (Table 2). To evaluate for heterogeneity in distribution and pattern of lung disease among individuals in this group, we next analyzed the upper, mid, and lower portions of the lungs on computed tomography (CT) scan through application of a modified National Emphysema Treatment Trial scoring system (Table 2) (Hersh et al., 2015) as well as quantification of lung CT densitometry (Table S1) (Onieva et al., 2016; Ross et al., 2009). While we did find classic lower lobe panlobular emphysema in some scans, we likewise noted significant heterogeneity in emphysema type and distribution (Tables 2 and S1). We additionally assembled test results to characterize the presence or absence and degree of liver disease for each donor, including biochemistry, transaminases, international normalized ratio, and platelet count together with elastography and biopsy results when available (Table 3). Elastography detected some degree of liver fibrosis in five of five PiZZ individuals tested with two of five having probable or definite cirrhosis.

Differentiation Capacity of AATD iPSCs to Disease-Relevant Lineages

To demonstrate the utility of patient-specific cells for disease modeling, we selected PBMC samples from our

Table 1. AATD Patient-Specific Repository

Line	Genotype	Sex	Age (years)	Line	Genotype	Sex	Age (years)	Line	Genotype	Sex	Age (years)
PiZZ1[a,b]	ZZ	M	44	CA-003[a]	ZZ	F	20	MO-005[a]	ZZ	F	57
PiZZ2[a,b]	ZZ	M	65	CA-004[a]	ZZ	M	70	MO-006[a]	ZZ	F	44
PiZZ3[a,b]	ZZ	M	65	CA-005[a]	ZZ	M	63	MO-007[a]	ZZ	F	63
PiZZ4[a]	ZZ	F	55	CA-006[a]	ZZ	M	45	MO-008[a]	ZZ	F	54
PiZZ5[a]	ZZ	F	57	CA-007[a]	ZZ	M	77	MO-009[a]	ZZ	F	63
PiZZ6[a,c]	ZZ	F	16	CA-008[a]	ZZ	M	58	MO-010[a]	ZZ	F	36
PiZZ7[a]	ZZ	F	62	CA-009[a]	ZZ	F	61	MO-011[a,c]	ZZ	M	53
PiZZ8[a]	ZZ	F	48	CA-010[a]	ZZ	F	31	MO-012[a]	ZZ	F	58
PiZZ9[a]	ZZ	F	69	CA-011[a]	ZZ	F	68	MO-013[a]	ZZ	F	57
PiZZ10[a]	ZZ	M	64	CA-012[a]	ZZ	F	53	MO-014[a]	ZZ	M	35
PiZZ11[a]	ZZ	F	35	CA-013[a]	ZZ	M	72	MO-015[a]	ZZ	F	60
PiZZ12[a]	ZZ	F	71	CA-014[a]	ZZ	M	72	MO-016[a]	ZZ	M	74
PiZZ13[a]	ZZ	M	49	CA-015[a]	ZZ	M	71	MO-017[a]	ZZ	M	68
PiZZ14[a]	ZZ	F	62	CA-016[a]	ZZ	M	55	MO-018[a]	ZZ	F	58
PiZZ15[a]	ZZ	F	52	CA-017[a]	ZZ	M	63	MO-019[a]	ZZ	F	54
PiZZ16[a]	ZZ	M	58	CA-018[a]	ZZ	F	70	MO-020[a]	ZZ	F	80
PiZZ17[a]	ZZ	M	61	CA-019[a]	ZZ	F	18	MO-021[a]	ZZ	M	60
PiZZ18[a]	ZZ	F	66	CA-020[a]	ZZ	F	45	MO-022[a]	ZZ	M	45
PiZZ19[a]	ZZ	F	31	CA-021[a]	ZZ	M	51	MO-023[a]	ZZ	M	67
PiZZ20[a]	ZZ	F	65	CA-022[a]	ZZ	M	59	MO-024[a]	ZZ	F	40
PiZZ21[a]	ZZ	F	71	CA-023[a]	ZZ	F	54	MO-025[a]	ZZ	F	51
PiZZ22[a]	ZZ	M	58	CA-024[a]	ZZ	M	45	MO-026[a]	ZZ	M	50
PiZZ23[a]	ZZ	M	68	CA-025[a]	ZZ	F	68	MO-027[a]	ZZ	F	50
PiZZ24[a]	ZZ	M	43	CA-026[a]	ZZ	M	62	MO-028[a]	ZZ	F	26
PiZZ25[a]	ZZ	F	38	CA-027[a]	ZZ	F	63	MO-029[a]	ZZ	M	37
PiZZ26[a]	ZZ	M	82	CA-028[a]	ZZ	F	42	MO-030[a]	ZZ	F	62
PiZZ27[a]	ZZ	F	51	CA-029[a]	ZZ	F	63	MO-031[a]	ZZ	F	76
PiZZ28[a]	ZZ	F	25	CA-030[a]	ZZ	F	72	MO-032[a]	ZZ	F	56
PiZZ29[a]	ZZ	F	52	MA-001[a]	ZZ	F	58	PiSZ1[a,b]	SZ	F	68
PiZZ30[a]	ZZ	F	19	MA-002[a,c]	ZZ	M	69	PiSZ2[a,b]	SZ	F	62
PiZZ31[a]	ZZ	F	72	MA-003[a]	ZZ	F	65	PiSZ3[a,b]	SZ	M	56
PiZZ32[a]	ZZ	M	59	MA-004[a]	ZZ	M	65	PiSZ4[a]	SZ	F	30
PiZZ33[a]	ZZ	M	64	MA-005[a]	ZZ	F	40	PiSZ5[a]	SZ	F	59
PiZZ34[a]	ZZ	F	58	MA-006[a]	ZZ	F	65	PiSZ6[a]	SZ	F	54

(Continued on next page)

Table 1. *Continued*

Line	Genotype	Sex	Age (years)	Line	Genotype	Sex	Age (years)	Line	Genotype	Sex	Age (years)
PiZZ35[a]	ZZ	F	49	MA-007[a]	ZZ	M	69	PiSZ7[a]	SZ	M	72
PiZZ36[a]	ZZ	M	55	MA-008[a]	ZZ	M	56	PiSZ8[a]	SZ	F	47
PiZZ37[a]	ZZ	F	59	MA-009[a]	ZZ	F	51	PiSZ9[a]	SZ	M	64
PiZZ38[a]	ZZ	F	68	MA-010[a]	ZZ	M	42	PiSZ10[a]	SZ	F	64
PiZZ39[a]	ZZ	F	71	MA-011[a,c]	ZZ	F	37	PiSS1[a]	SS	M	42
PiZZ100[b,d]	ZZ	F	67	MA-012[a]	ZZ	M	54	PiSS2[a]	SS	M	51
PiZZ101[b,d]	ZZ	F	65	MA-013[a]	ZZ	M	44	PiZMh1[a,b]	$ZM_{Heerlen}$	F	76
PiZZ102[b,d]	ZZ	F	51	MA-014[a]	ZZ	M	32	PiZMh2[a]	$ZM_{Heerlen}$	M	37
PiZZ103[b,d]	ZZ	F	61	MA-015[a]	ZZ	M	58	PiFZ1[a,b]	FZ	M	56
CBZ1[a,b]	ZZ	M	NA	MA-016[a]	ZZ	F	23	PiBB1[b,d]	$Q0_{Bolton}Q0_{Bolton}$	M	46
CBZ3[a,b]	ZZ	M	NA	MA-017[a]	ZZ	M	55	$PiZV_{Grantspass}1$[a]	$ZV_{Grantspass}$	F	67
CBZ4[a,c]	ZZ	F	NA	MA-018[a]	ZZ	M	36	$PiZQ0_{Newcity}1$[a]	$ZQ0_{Newcity}$	F	71
CBZ5[a,c]	ZZ	M	NA	MA-019[a]	ZZ	F	54	PiMZ2[a]	MZ	F	79
CBZ6[a,c]	ZZ	F	NA	MA-020[a]	ZZ	M	71	PiMZ3[a]	MZ	M	59
CBZ7[a,c]	ZZ	M	NA	MA-022[a]	ZZ	F	45	PiMZ4[a]	MZ	F	64
CBZ8[a,c]	ZZ	F	NA	MA-023[a]	ZZ	M	58	PiMZ5[a]	MZ	M	38
CBZ9[a,c]	ZZ	M	NA	MA-025[a]	ZZ	F	63	PiMZ6[a]	MZ	M	53
CBZ12[a,c]	ZZ	M	NA	MA-026[a]	ZZ	M	58	PiMZ7[a]	MZ	M	50
CBZ13[a,c]	ZZ	M	NA	MO-001[a]	ZZ	F	71	PiMZ8[a]	MZ	M	37
CBZ14[a,c]	ZZ	M	NA	MO-002[a]	ZZ	M	40	PiMZ9[a]	MZ	M	53
CA-001[a]	ZZ	M	47	MO-003[a]	ZZ	M	68	PiMZ10[a]	MZ	F	51
CA-002[a]	ZZ	M	62	MO-004[a]	ZZ	M	50	PiMS1[a]	MS	F	41

Summary of the 168 peripheral blood or skin fibroblast samples obtained from subjects with *SERPINA1* mutations. Included within the repository are samples representative of common disease-causing variants (S,Z) as well as rare and novel mutations. Twenty-eight samples (highlighted) have been reprogrammed into established iPSC lines. See also Figures S1 and S2.

PBMC, peripheral blood mononuclear cell; M, male; F, female; NA, not available.
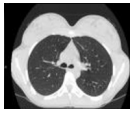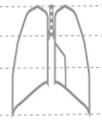[a]PBMC.
[b]STEMCCA.
[c]Sendai virus.
[d]Skin fibroblast.
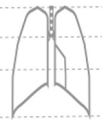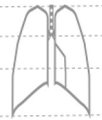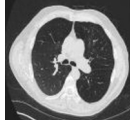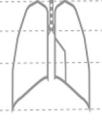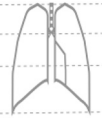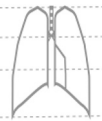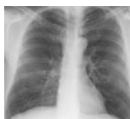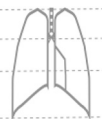
repository for reprogramming to generate iPSCs. In addition to the 10 featured samples detailed above, we reprogrammed 18 samples representing a variety of *SERPINA1* deficiency allele combinations (Figure 1; Table 1). Each iPSC line was confirmed to have a normal karyotype and to express markers of pluripotency before proceeding to directed differentiation experiments (Figures S1 and S2; additional pluripotency staining can be found at https://stemcellbank.bu.edu). We have previously established directed differentiation protocols to generate iPSC-derived hepatic cells (iHeps) (Wilson et al., 2015; Kaser-man and Wilson, 2017; Reeves et al., 2018), and to derive either proximal or distal differentiated lung lineages (Hawkins et al., 2017; Jacob et al., 2017; McCauley et al., 2017, 2018) for disease modeling and assessment of drug responsiveness. To apply these protocols to each of the ten featured iPSC lines, a single vial of cryopreserved iPSCs representing each line was thawed, expanded, and split to accomplish parallel liver- and lung-directed differentiation (Figure 2A). Undifferentiated iPSCs were first patterned into definitive endoderm, the germ layer from which both the lung and liver derive embryologically.
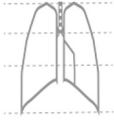
Table 2. Demographic and Clinical Pulmonary Characteristics

Subject ID	Genotype, Age (years)	FEV1	FEV1/FVC	DLCO	CXR Image	CT Image	CT Read	CT Score
PiZZ6	ZZ, 16	3.40 (108%)	85%	92%			no emphysema	0 / 0 / 0
MA-011	ZZ, 37	2.43 (85%)	78%	data unavailable			no emphysema	0 / 0 / 0
PiZZ1	ZZ, 44	2.60 (75%)	63%	79%			diffuse cystic lung disease. No emphysema	0 / 0 / 0
PiZZ2	ZZ, 65	0.59 (18%)	21%	21%			moderate centrilobular & paraseptal emphysema	2 / 3 / 3
PiZZ3	ZZ, 65	1.44 (48%)	52%	data unavailable			moderate centrilobular emphysema	2 / 3 / 3
PiZZ100	ZZ, 67	0.91 (39%)	46%	31%			panlobular emphysema	1 / 2 / 4
MA-002	ZZ, 69	1.82 (68%)	39%	66%			moderate centrilobular emphysema	2 / 4 / 3
PiSZ3	SZ, 56	0.81 (24%)	19%	40%	data unavailable	data unavailable	emphysema[a]	data unavailable

(Continued on next page)

Table 2. *Continued*

Subject ID	Genotype, Age (years)	FEV1	FEV1/FVC	DLCO	CXR Image	CT Image	CT Read	CT Score	
PiSZ2	SZ, 62	2.09 (94%)	59%	83%			mild diffuse centrilobular emphysema	1 1 1	
PiSZ1	SZ, 68	0.55 (21%)	32%	21%			advanced destructive centrilobular emphysema	4 3 3	

PFT, pulmonary function tests; FEV1, forced expiratory volume in 1 s in liters (percent predicted); FVC, forced vital capacity; DLCO, diffusion capacity for carbon monoxide in percent predicted; CXR, chest X-ray; CT, computed tomography.
CT score: 0, no emphysema; 1, mild emphysema; 2, moderate emphysema; 3, severe emphysema; 4, very severe emphysema.
See also Table S1.
[a]Clinical report.

These cells were then further specified through sequential exposure to lineage-specific growth factors to derive either iHeps or lung progenitors (Figures 2A, 2B, and S3). We sorted cells on day 15 of our lung-directed differentiation protocol based on the cell surface marker profile, CD47^{hi}/CD26^{lo}, which enriches for lung progenitor cells expressing the earliest known lung lineage marker, NKX2-1 (Hawkins et al., 2017). This sort strategy achieved an enrichment in NKX2-1+ putative lung progenitors of >85% in eight out of nine iPSC lines tested (mean 87.6% ± 11.2%) from a pre-sort mean NKX2-1 percentage of 39.5% ± 14.3% (Figure S3). These lung progenitors can be further differentiated to either distal (Gotoh et al., 2014; Jacob et al., 2017) or proximal lung lineages for disease modeling of specific compartments (Firth et al., 2015; McCauley et al., 2017).

iHeps differentiated from these ten featured iPSC lines in these experiments consistently acquired a characteristic hepatocyte-like morphology (Wilson et al., 2015). Intracellular AAT, quantified by mean fluorescence intensity (MFI), demonstrated significant AAT protein retention with an average MFI of 427.13 ± 88.64 (Figures 2B, 2C, and S3). We and others have previously found hepatic-directed differentiation of iPSCs to be efficient across multiple lines but with some line-to-line variability (Ogawa et al., 2013; Pashos et al., 2017; Warren et al., 2017; Wilson et al., 2015), consistent with the differentiation efficiencies we observed across our ten featured lines. Together, these findings demonstrate the ability of featured iPSC lines to differentiate into multiple downstream lineages relevant to AATD disease pathogenesis.

Transcriptional Profiling of iPSC-Derived Lung Progenitors, iHeps, and Primary Human Hepatocytes

We next profiled the global transcriptomes of both iHeps and lung progenitors derived from the ten featured lines. We used digital gene expression (DGE), a platform for high-fidelity RNA sequencing (Cacchiarelli et al., 2015). In addition to differentiated iPSC-derived cell types, we collected RNA from undifferentiated iPSCs and from a panel of primary adult human hepatocytes (PHH) for comparison (Figure 3A). Principal-component analysis (PCA) of the sequencing data revealed four distinct groups (Figure 3B), with undifferentiated and lung progenitor samples clustering separately from both PHH and iHeps. PHH and iHep transcriptomes displayed a similar first-principal-component variance (Figure 3B) consistent with less transcriptomic variance among hepatic cells of primary or engineered origin, relative to other cell types. We next analyzed expression levels of selected genes known to mark hepatic, lung, and undifferentiated lineages (Figure 3C). Using empirical Bayes moderated t-statistical analysis, the expression of specific key pluripotency-associated genes, including *POU5F1* (OCT4) and *NANOG*, were significantly upregulated in undifferentiated iPSCs (false discovery rate [FDR] < 0.001), while *NKX2-1* and *CPM*, known markers of iPSC-derived lung progenitor cells (Gotoh et al., 2014; Hawkins et al., 2017), as well as markers of immature fetal lung, such as *SOX9*, *GATA6*, and *ELF5* (Hawkins et al., 2017; Nikolic et al., 2017), were significantly upregulated in the iPSC-lung progenitors (FDR < 0.001). Conversely, established hepatic lineage genes, such as *TTR*, *SERPINA1*, and *ALB* (Wilson et al.,
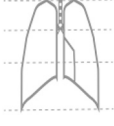
Table 3. Demographic and Clinical Hepatic Characteristics

Subject ID	Genotype, Age (years)	ALT (0–44 IU/L)	Total Bilirubin (0–1.2 mg/dL)	Albumin (3.5–5.5 g/dL)	Platelets (150–379 × 10³/μL)	INR (0.8–1.2)	Non-invasive Imaging Findings RUQ US/VCTE (Fibrosis Score)	Biopsy Findings
PiZZ6	ZZ, 16	19	<0.1	4.6	368	0.91	mild hepatomegaly	Ishak fibrosis 4, PAS-D+ hepatocytes zone 1
MA-011	ZZ, 37	34	0.6	4.7	321	0.93	F2 fibrosis	Ishak fibrosis 1, PAS-D+ hepatocytes zone 2
PiZZ1	ZZ, 44	46	0.9	3.0	121	1.35	cirrhosis, splenomegaly, ascites	data unavailable
PiZZ2	ZZ, 65	22	1.0	3.8	180	1.10	data unavailable	data unavailable
PiZZ3	ZZ, 65	41	0.4	3.5	259	1.30	data unavailable	data unavailable
PiZZ100	ZZ, 67	23	0.5	4.3	301	1.00	probable cirrhosis	data unavailable
MA-002	ZZ, 69	29	0.5	4.4	268	1.09	F1 fibrosis	Ishak fibrosis 0, PAS-D+ hepatocytes zones 1 and 2
PiSZ3	SZ, 56	24	0.2	3.5	303	1.00	data unavailable	data unavailable
PiSZ2	SZ, 62	24	0.9	4.5	228	0.91	data unavailable	data unavailable
PiSZ1	SZ, 68	21	0.3	3.7	201	data unavailable	data unavailable	data unavailable

ALT, alanine aminotransferase; INR, international normalized ratio; RUQ US, right upper quadrant ultrasound; VCTE, vibration-controlled transient elastography.

VCTE fibrosis score: F0, no scarring; F1, mild scarring; F2, moderate scarring; F3, severe scarring; F4, cirrhosis.

Ishak fibrosis score: 0, no fibrosis; 1, fibrous expansion of some portal areas; 2, fibrous expansion of most portal areas; 3, fibrous expansion of most portal areas with occasional portal to portal bridging; 4, fibrous expansion of portal areas with marked portal-portal bridging; 5, marked bridging with occasional nodules; 6, cirrhosis.

2015), were upregulated (FDR < 0.001) in both iHeps and PHH consistent with the PCA groupings.

To identify the biological or pathogenic pathways that characterize our iHeps and iPSC-lung progenitors we used gene set variation analysis, a non-parametric, unsupervised method for estimating variation of gene set enrichment through the samples of an expression dataset (Figure 3D). This analysis demonstrated enrichment of relevant organ-specific hallmark pathways for each of the groups studied (Liberzon et al., 2015). For example, iPSC-lung progenitors exhibited enrichment of "Lung Morphogenesis," "Alveolar Development," "Lung Epithelium Development," and "Lung Cell Differentiation" pathways, while "Regulation of Hepatocyte Proliferation" and "Liver Regeneration" pathways were enriched in iHeps. *SERPINA1* is one of the most highly upregulated genes in iHeps relative to undifferentiated controls (Wilson et al., 2015). Consistent with this expression pattern and the known contribution of the ZAAT variant to hepatic injury, AATD iHeps also demon-strated higher enrichment scores within pathways associated with fibrosis and cirrhosis (e.g., transforming growth factor β signaling, epithelial-mesenchymal transition, hepatocyte apoptotic process) in comparison with PHH, a finding with potential relevance to AAT liver disease modeling.

The ability to assess the efficiency of hepatic differentiation between different iPSC lines and across experiments is a recognized challenge in iPSC-directed differentiation protocols (Wilson et al., 2015; Pashos et al., 2017). To compare relative efficiencies for each of the 10 ZAAT iHep differentiations, we assigned an individual hepatic enrichment score using a panel of 30 genes significantly upregulated in PHH compared with undifferentiated iPSCs (Figure 3E; Table S2). Application of this score revealed a moderate degree of variability in hepatic enrichment among iHep lines, consistent with our experience and published reports describing line-to-line variability in directed differentiation protocols (Pashos
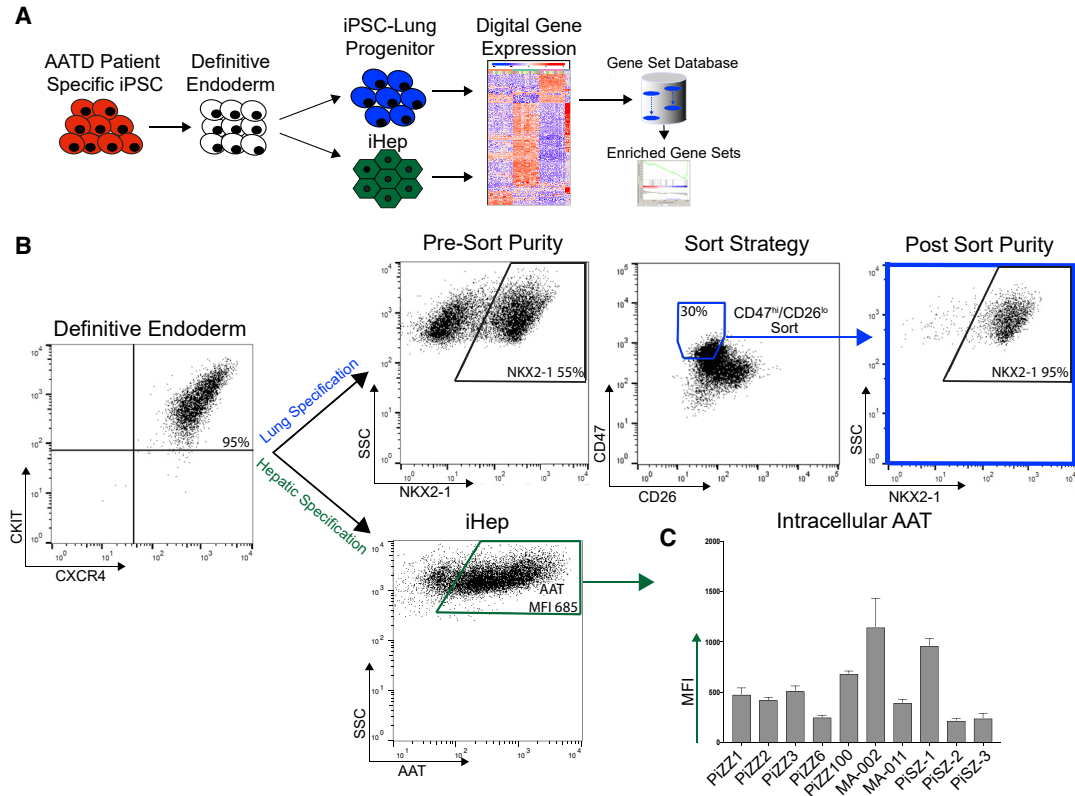
Figure 2. Directed Differentiation of AATD Patient-Specific iPSCs into Endodermal Lineages

(A) Schematic demonstrating the specification of AATD patient-derived iPSCs into the two most disease-relevant endodermal lineages.

(B) Representative flow cytometric analysis using stage-specific markers at key directed differentiation time points, including definitive endoderm (day 3 or 4), lung progenitors (day 15), and iHeps (day 26).

(C) MFI of intracellular AAT for all 10 AATD lines. n = 3 independent experiments. Data are represented as mean ± SEM.

See also Figure S3.

et al., 2017). To test the specificity of the score we likewise applied it to iPSC-lung progenitors and found reduced hepatic enrichment relative to iHep comparators as expected (average 0.5695 ± .024; p < 0.0001) (Figure 3F).

CRISPR/Cas9 Gene Editing of the *SERPINA1* Locus in AATD Patient-Derived iPSCs

To isolate the cellular effects that result directly from endogenous ZAAT expression within a single genetic background, we next applied the CRISPR/Cas9 endonuclease system to achieve scarless correction of the Z mutation (Figures 4 and S4). Using this approach, we were able to target multiple PiZZ iPSC lines to generate corrected, syngeneic PiMM daughter lines achieving an overall biallelic correction efficiency of 6% (Figure 4C). After gene correction was confirmed via Sanger sequencing, edited lines underwent repeat karyotyping and staining for markers of pluripotency (data not shown). To evaluate the downstream effects of gene correction, syngeneic PiZZ and PiMM iPSC

lines were then differentiated in parallel to generate iHeps for comparison. As expected, edited PiMM iHeps displayed reduced levels of intracellular AAT protein accumulation together with an increase in secreted AAT in comparison with their parental PiZZ iHeps (Figures 4D–4G).

DISCUSSION

iPSC technology and the associated ability to derive disease-associated cell types in a specific genetic context has provided a new avenue to study the contribution of gene variants to disease. Their unlimited capacity as a source of differentiated cell types together with their amenability to genetic manipulation further underscore the potential utility of the iPSC model to elucidate cellular disease mechanisms. AATD is characterized by significant inter-individual variability in disease manifestation, suggesting the need for a model that captures the genetic heterogeneity of the patient population. Therefore, we have generated a
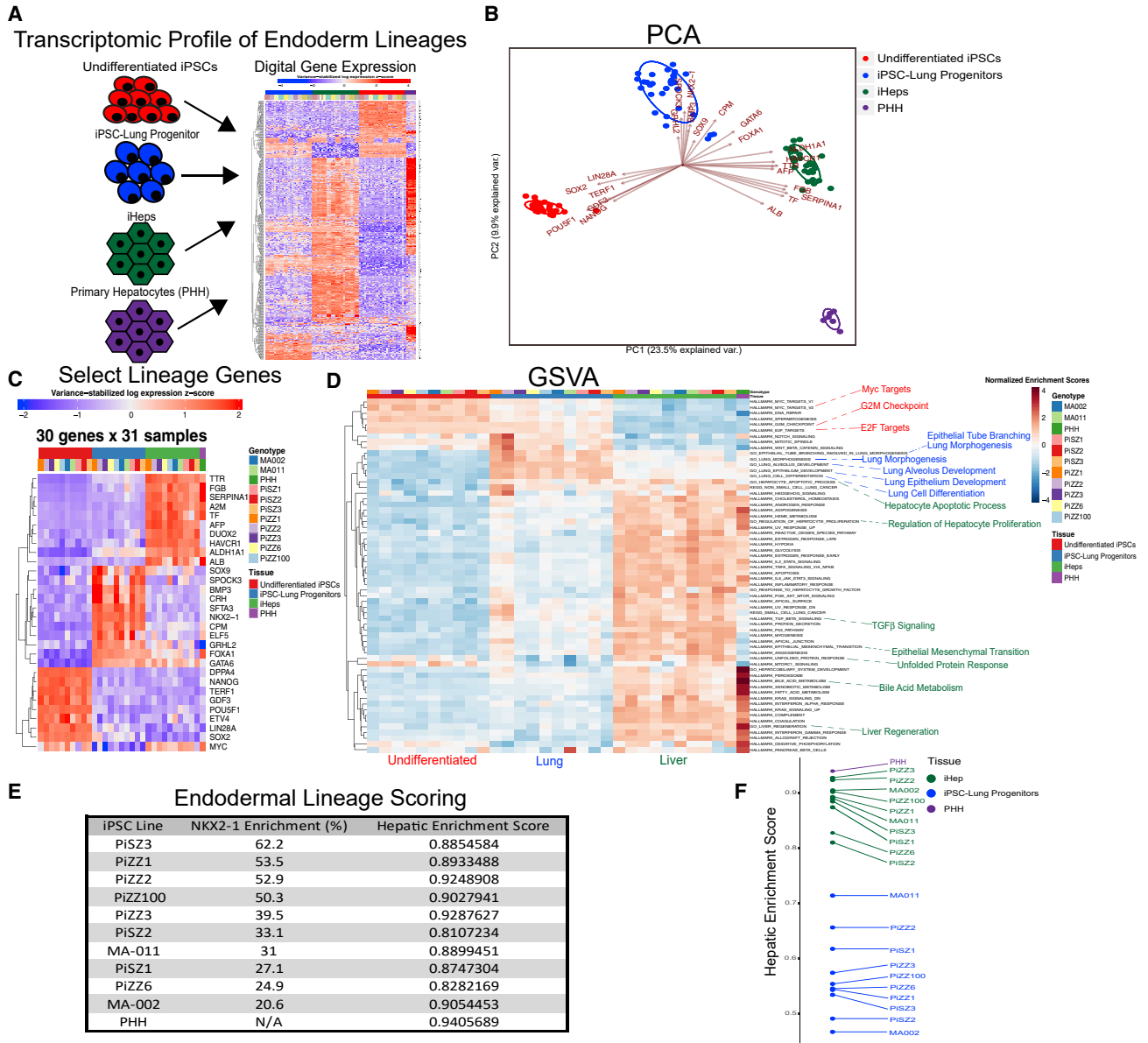
Figure 3. Transcriptomic Profile of AATD Patient-Derived iPSC-Lung Progenitors and Hepatic Cells

(A) Schematic demonstrating transcriptomic profiling from 10 AATD iPSC lines using DGE.

(B) PCA demonstrates samples clustered predominantly by cell type.

(C) Heatmap of selected lineage-specific markers across iPSC-derived and primary samples.

(D) Gene set variation analysis demonstrates enrichment within relevant organ-specific hallmark pathways for each group.

(E) Quantification of lung and hepatic differentiation efficiency for each iPSC line based on percent enrichment for NKX2-1 and application of a 30-gene transcriptomic signature of hepatic enrichment.

(F) Ranking of all samples by hepatic enrichment score.

See also Table S2.

repository of iPSCs from numerous patients with *SERPINA1* mutations to allow the generation and study of disease-affected cell types in multiple genetic backgrounds.

It is likely that additional as-of-yet undefined polymorphisms in disease-modifying genes contribute to heteroge-

neity of outcomes in AATD patients observed in clinical practice. The ability to apply this model for either discovery or validation of additional genetic modifiers will require careful clinical phenotyping to correctly classify and characterize clinical outcomes of interest. For this reason, the
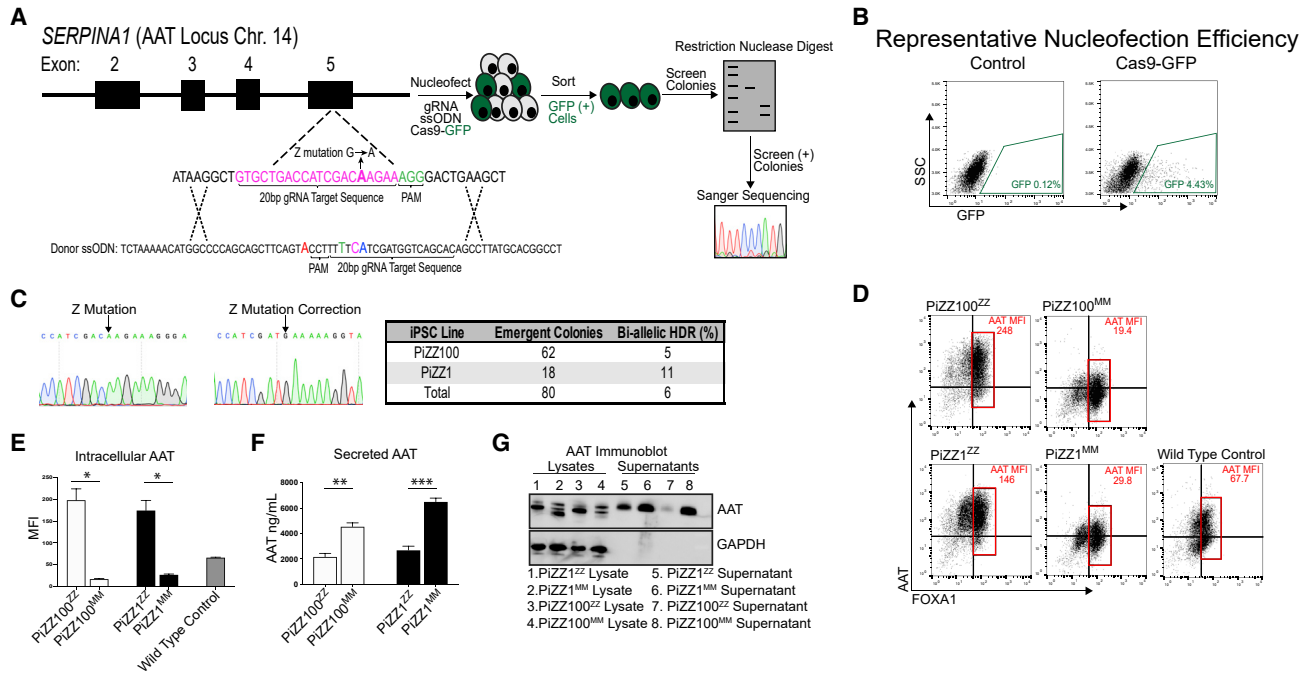
Figure 4. Scarless Gene Correction of the Z Mutation in AATD Patient-Derived iPSCs Using CRISPR/Cas9

(A) Targeting strategy for the Z mutation located within exon five of SERPINA1. A 70-bp single-stranded oligodeoxynucleotide (ssODN) repair template sequence is shown with the wild-type sequence highlighted in pink, the new ClaI restriction enzyme site in blue, and silent mutations to reduce CRISPR targeting of the donor sequence in green and red.

(B) Representative fluorescence-activated cell sorting plots demonstrating nucleofection efficiency in AATD iPSCs.

(C) Efficiency of biallelic homology-directed repair across genetically distinct ZZ AATD iPSCs.

(D) Flow cytometry of fixed, permeabilized iHeps demonstrates significant reduction of intracellular AAT protein within CRISPR-corrected syngeneic PiMM iHeps.

(E) MFI of AAT in syngeneic PiZZ and PiMM iHeps.

(F) ELISA of total secreted AAT levels from syngeneic PiZZ and PiMM iHep supernatants.

(G) Immunoblot probed with anti-AAT antibody demonstrates reduced intracellular levels of the native 52-kDA AAT protein with increased levels of secreted mature 55-kDa AAT protein in the syngeneic PiMM relative to PiZZ iHeps. n = 3 independent experiments. Data represented as mean ± SEM. *$p < 0.05$, **$p < 0.01$, ***$p < 0.001$ by two-tailed t test.

See also Figure S4.

clinical database compiled in these studies and associated with this repository greatly enhances its potential value. This database can be interrogated upon request to identify samples representative of specific clinical phenotypes. In addition to association of biological samples with clinical data, iPSC repositories, such as the one described, here possess other important attributes that distinguish them and their reagents from those held by individual investigators. These include curated selection of iPSC lines to represent significant clinical phenotypes, maintenance of quality control standards to ensure that constituent iPSCs do not harbor significant karyotypic abnormalities, documentation of donor consents that allow sharing of lines and associated clinical data with academic and industry-associated investigators, and streamlined material transfer agreements that minimize administrative barriers to sharing (Park et al., 2017).

In these studies, we defined the functional ability of each characterized iPSC line to differentiate into multiple disease-relevant lineages. The capacity to generate multiple differentiated lineages from each line allows the experimental modeling of multiorgan diseases in a genetically controlled fashion, a feature that separates this model system from heterologous cell lines (Giadone et al., 2019). Published work delineating protocols for deriving lung progenitor cells and their differentiated progeny have largely been based on a limited number of pluripotent stem cell lines (Gotoh et al., 2014; Hawkins et al., 2017; Huang et al., 2013; Jacob et al., 2017; Longmire et al., 2012; McCauley et al., 2017, 2018; Mou et al., 2012). While protocol optimization for specific lines can enhance differentiation efficiency, this work demonstrates the application of a single differentiation protocol applied to numerous donor iPSC lines, each of which efficiently generated

lung progenitor cells, precursor cells for all lung epithelium that can be subsequently used to model disease in the proximal and distal lung (Hawkins et al., 2017; Jacob et al., 2017; Longmire et al., 2012; McCauley et al., 2017, 2018).

In addition to characterizing PiZZ patient cells in our experiments, we have likewise included PiSZ iPSCs heterozygous for the Z and S mutations, an allele combination not associated with high levels of polymerization and not known to confer significant additional risk for the development of liver disease (American Thoracic Society and European Respiratory Society, 2003; Tan et al., 2014). In addition, we chose to profile multiple genetically distinct primary hepatocyte samples as comparators to derive a more robust primary cell expression profile that accounts for known inter-individual differences in gene expression (Pashos et al., 2017).

Directed differentiation protocols for the derivation of hepatic cells from iPSCs and their application to model liver disease are well established (Rashid et al., 2010; Segeritz et al., 2018; Smith et al., 2015; Wilson et al., 2015). A significant hurdle in these protocols, however, has been the ability to compare the relative efficiency of differentiation across experiments as liver-specific lineage markers, such as *AFP*, are expressed in early hepatoblasts while more mature hepatocyte genes, such as *ASGR1*, mark only a minority of cells in current differentiation protocols (Warren et al., 2017). To quantify differences in the differentiation efficiency for iHeps generated in our studies, we applied the primary hepatocyte gene expression profile to generate a signature of relative hepatic enrichment using an unbiased, computational approach. Application of this signature identified modest differences across the ten profiled genetic backgrounds. Whether these observations result in differences in meaningful functional outcomes will require additional testing to determine.

Previous reports have demonstrated the application of gene-editing technologies to generate biallelic correction of the Z mutation (Choi et al., 2013; Smith et al., 2015; Yusa et al., 2012). The ability to generate such isogenic, gene-corrected variants is important to control for genetic heterogeneity in the conduct of experiments evaluating the contribution of specific mutations to disease pathogenesis. Here, we illustrate a detailed, reproducible approach to CRISPR/Cas9-based editing of the Z mutation using open source reagents that we have applied to multiple PiZZ iPSC lines in our repository. These edited lines, together with other lines described here, are now freely available for sharing with academic and industry researchers.

In summary, we have created a repository of iPSCs with detailed associated clinical characterization from individuals with AATD. Through systematic characterization of the capacity of selected lines to generate disease-associated cell types, we have sought to illustrate and enhance the utility of this repository to interested investigators. The lines characterized in this study were created with donor consent explicitly allowing for sharing and commercialization, are available by request, and can be found online at https://stemcellbank.bu.edu. We are hopeful that the repository and its constituent lines will thus be applied to advance understanding of AATD-associated lung and liver disease pathogenesis and thereby benefit AATD patients.

EXPERIMENTAL PROCEDURES

Subjects
The recruitment of human subjects and all iPSC studies were approved by the Boston University institutional review board (BUMC IRB protocols H-29791, H-32506, and H-33064). Subjects were recruited from clinical practice at the Alpha-1 Foundation-associated patient support group and patient education meetings and in association with clinical studies of AATD patients (ClinicalTrials.gov identifiers: NCT02014415; NCT01379469). At the time of recruitment demographic and detailed clinical data were collected and managed using REDCap electronic data capture tools hosted at Boston University (Harris et al., 2009, 2019).

iPSC Line Generation and Maintenance
Derivation of iPSC lines in the repository was performed as described previously (Choi et al., 2014; Somers et al., 2010; Sommer et al., 2009; Wilson et al., 2015). In brief, each iPSC line was generated from either human dermal fibroblasts or PBMCs. After expansion, cells were reprogrammed using either the STEMCCA lentiviral reprogramming vector (Somers et al., 2010) or Sendai virus CytoTune2 Reprogramming Kit (Thermo Fisher Scientific). Following reprogramming, each line was maintained on murine embryonic fibroblast feeders with knockout serum replacement supplemented medium, or in feeder free conditions with mTeSR-1 medium (STEMCELL Technologies).

iPSC Sharing and Distribution
To facilitate sharing of iPSC lines in the repository, an online catalog was created with the URL https://stemcellbank.bu.edu. This catalog includes detailed information pertaining to each repository iPSC line, including but not limited to genotype, race/ethnicity, sex, age at sample collection, karyotype, short tandem repeat analysis, pluripotency characterization, testing for residual Sendai virus, associated gene-edited lines, and links to associated genomic datasets. Of note, iPSC lines are only made routinely available for distribution once they have undergone this detailed quality control processing.

iPSC-Derived Lung Progenitor Directed Differentiation
As described previously (Jacob et al., 2017; McCauley et al., 2018), NKX2-1+ lung progenitors were generated from iPSCs as follows: Cells were patterned into definitive endoderm using the STEMdiff Definitive Endoderm Kit (STEMCELL Technologies) as per the manufacturer's instructions. Cells were further differentiated using

stage-specific factors to generate first anterior foregut endoderm and then iPSC-lung progenitors. On day 15 of differentiation, primordial lung progenitor cells were sorted based on CD47^{hi}/CD26^{lo} gating (Hawkins et al., 2017).

iHep Generation

iPSC-directed differentiation toward the hepatic lineage was performed using our previously published protocol (Kaserman and Wilson, 2017; Wilson et al., 2015). In brief, cells were patterned into definitive endoderm using the STEMdiff Definitive Endoderm Kit as per the manufacturer's instructions. Cells were passaged on day 5 of differentiation and then cultured for an additional 21 days using stage-specific growth factors to specify the hepatic lineage and induce maturation. Detailed protocols for derivation of iPSC lung and hepatic cells are freely accessible at: https://www.bu.edu/dbin/stemcells/protocols.php.

PHH

Commercially available, cryopreserved PHH (human plateable, induction qualified) were obtained from Thermo Fisher Scientific. Single vials containing 8–14 × 10^6 cells were obtained from six genetically distinct lots and thawed as per the manufacturer's instructions. Cells (2 × 10^6) were used to seed four type I collagen-coated wells in 24-well format to verify viability; the remaining cells were immediately pelleted at the time of thaw and lyzed in QIAzol Reagent (QIAGEN) for RNA sequencing.

Fluorescence-Activated Cell Sorting Analysis

Efficiency of definitive endoderm induction was quantified using CD184-PE (STEMCELL Technologies) and CD117-APC (Thermo Fisher Scientific) antibodies. To quantify intracellular protein content, fixed and permeabilized iHeps were stained using anti-human AAT (Santa Cruz Biotechnologies) and anti-human FOXA1 (Santa Cruz Biotechnologies) antibodies followed by anti-mouse IgG1-Alexa Fluor 647 (Jackson ImmunoResearch) and IgG2a-DyLight 488 (Jackson ImmunoResearch) antibodies (Wilson et al., 2015).

RNA Sequencing

Total RNA was isolated using an miRNeasy kit (QIAGEN) as per the manufacturer's instruction. For DGE the concentrations of all samples were normalized and sent to the Broad Institute for library construction and sequencing (Cacchiarelli et al., 2015; Park et al., 2017). Reads were then aligned to the ENSEMBL human reference genome. The count matrix was filtered and normalized to facilitate linear model fitting and differential expression testing. A liver enrichment score was derived by identifying differentially expressed genes between PHH and undifferentiated iPSCs.

CRISPR-Based Editing of Z Mutation

The CRISPR/Cas9 endonuclease system was utilized to induce scarless correction of the "Z" mutation in the *SERPINA1* gene. A 70 bp single-stranded oligodeoxynucleotide repair template was synthesized (Integrated DNA Technologies) and delivered along with a single plasmid containing both the gRNA and Cas9-2A-GFP sequence via nucleofection (Lonza) to undifferentiated iPSCs. Af-

ter 48 h, GFP+ cells were sorted and sparsely plated to achieve clonal outgrowth. Colonies were then screened for repair template incorporation and were gene sequence confirmed via DNA sequencing.

ELISA

Secreted AAT was quantified from AATD iHep supernatants using the human alpha-1-antitrypsin ELISA quantification kit (GenWay Biotech) as per the manufacturer's instructions.

Western/Immunoblot

Cell protein lysates and supernatants were collected as described previously (Wilson et al., 2015), denatured, and run on a 4%–12% Bis-Tris gel in MOPS SDS buffer using the NuPAGE system (Invitrogen). Proteins were transferred to a polyvinylidene fluoride membrane. Membranes were probed with antibodies against AAT (Santa Cruz Biotechnologies) and GAPDH (EMD Millipore). Signal was detected using goat anti-mouse-conjugated horseradish peroxidase (Bio-Rad) and imaged on an LAS-4000 chemiluminescent imager (Fuji).

Data and Code Availability

The GEO accession number for the DGE data reported in this paper is GSE140732.

REFERENCES

American Thoracic Society; European Respiratory Society (2003). American Thoracic Society/European Respiratory Society statement: standards for the diagnosis and management of individuals with alpha-1 antitrypsin deficiency. Am. J. Respir. Crit. Care Med. *168*, 818–900.

Cacchiarelli, D., Trapnell, C., Ziller, M.J., Soumillon, M., Cesana, M., Karnik, R., Donaghey, J., Smith, Z.D., Ratanasirintrawoot, S., Zhang, Z., et al. (2015). Integrative analyses of human reprogramming reveal dynamic nature of induced pluripotency. Cell *162*, 412–424.

Choi, I.Y., Lim, H., and Lee, G. (2014). Efficient generation human induced pluripotent stem cells from human somatic cells with Sendai-virus. J. Vis. Exp. *86*, 1–9.

Choi, S.M., Kim, Y., Shim, J.S., Park, J.T., Wang, R.-H., Leach, S.D., Liu, J.O., Deng, C., Ye, Z., and Jang, Y.-Y. (2013). Efficient drug screening and gene correction for treating liver disease using patient-specific stem cells. Hepatology *57*, 2458–2468.

Eriksson, S. (1964). Pulmonary emphysema and alpha1-antitrypsin deficiency. Acta Med. Scand. *175*, 197–205.

Firth, A.L., Menon, T., Parker, G.S., Qualls, S.J., Lewis, B.M., Ke, E., Dargitz, C.T., Wright, R., Khanna, A., Gage, F.H., et al. (2015). Functional gene correction for cystic fibrosis in lung epithelial cells generated from patient iPSCs. Cell Rep. *12*, 1385–1390.

Giadone, R.M., Rosarda, J.D., Akepati, P.R., Thomas, A.C., Boldbaatar, B., James, M.F., Wilson, A.A., Sanchorawala, V., Connors, L.H., Berk, J.L., et al. (2019). A library of ATTR amyloidosis patient-specific induced pluripotent stem cells for disease modelling and in vitro testing of novel therapeutics. Amyloid *25*, 148–155.

Gotoh, S., Ito, I., Nagasaki, T., Yamamoto, Y., Konishi, S., Korogi, Y., Matsumoto, H., Muro, S., Hirai, T., Funato, M., et al. (2014). Generation of alveolar epithelial spheroids via isolated progenitor cells from human pluripotent stem cells. Stem Cell Reports *3*, 394–403.

Harris, P.A., Taylor, R., Thielke, R., Payne, J., Gonzalez, N., and Conde, J.G. (2009). Research electronic data capture (REDCap)—a metadata-driven methodology and workflow process for providing translational research informatics support. J. Biomed. Inform. *42*, 377–381.

Harris, P.A., Taylor, R., Minor, B.L., Elliott, V., Fernandez, M., O'Neal, L., McLeod, L., Delacqua, G., Delacqua, F., Kirby, J., et al. (2019). The REDCap consortium: building an international community of software partners. J. Biomed. Inform. *95*, 103208.

Hawkins, F., Kramer, P., Jacob, A., Driver, I., Thomas, D.C., McCauley, K.B., Skvir, N., Crane, A.M., Kurmann, A.A., Hollenberg, A.N.,

et al. (2017). Prospective isolation of NKX2-1-expressing human lung progenitors derived from pluripotent stem cells. J. Clin. Invest. *127*, 2277–2294.

Hersh, C.P., Washko, G.R., Jacobson, F.L., Gill, R., Estepar, R.S.J., Reilly, J.J., and Silverman, E.K. (2015). Interobserver variability in the determination of upper lobe-predominant emphysema. Chest *131*, 424–431.

Huang, S.X.L., Islam, M.N., O'Neill, J., Hu, Z., Yang, Y.-G., Chen, Y.-W., Mumau, M., Green, M.D., Vunjak-Novakovic, G., Bhattacharya, J., et al. (2013). Efficient generation of lung and airway epithelial cells from human pluripotent stem cells. Nat. Biotechnol. *32*, 84–91.

Jacob, A., Morley, M., Hawkins, F., McCauley, K.B., Jean, J.C., Heins, H., Na, C.-L., Weaver, T.E., Vedaie, M., Hurley, K., et al. (2017). Differentiation of human pluripotent stem cells into functional lung alveolar epithelial cells. Cell Stem Cell *21*, 472–488.

Kaserman, J.E., and Wilson, A.A. (2017). Protocol for directed differentiation of human induced pluripotent stem cells (iPSCs) to a hepatic lineage. Methods Mol. Biol. *1639*, 151–160.

Laurell, C.-B., and Eriksson, S. (1963). The electrophoretic α1-globulin pattern of serum in α1-antitrypsin deficiency. Scand. J. Clin. Lab. Invest. *15*, 132–140.

Leung, A., Nah, S.K., Reid, W., Ebata, A., Koch, C.M., Monti, S., Genereux, J.C., Wiseman, R.L., Wolozin, B., Connors, L.H., et al. (2013). Induced pluripotent stem cell modeling of multisystemic, hereditary transthyretin amyloidosis. Stem Cell Reports *1*, 451–463.

Lieberman, J., Winter, B., and Sastre, A. (1986). Alpha 1-antitrypsin Pi-types in 965 COPD patients. Chest *89*, 370–373.

Liberzon, A., Birger, C., Thorvaldsdottir, H., Ghandi, M., Mesirov, J.P., and Tamayo, P. (2015). The molecular signatures database hallmark gene set collection. Cell Syst. *1*, 417–425.

Longmire, T.A., Ikonomou, L., Hawkins, F., Christodoulou, C., Cao, Y., Jean, J.C., Kwok, L.W., Mou, H., Rajagopal, J., Shen, S.S., et al. (2012). Efficient derivation of purified lung and thyroid progenitors from embryonic stem cells. Cell Stem Cell *10*, 398–411.

McCauley, K.B., Hawkins, F., Serra, M., Thomas, D.C., Jacob, A., and Kotton, D.N. (2017). Efficient derivation of functional human airway epithelium from pluripotent stem cells via temporal regulation of Wnt signaling. Cell Stem Cell *20*, 844–857.

McCauley, K.B., Hawkins, F., and Kotton, D.N. (2018). Derivation of epithelial-only airway organoids from human pluripotent stem cells. Curr. Protoc. Stem Cell Biol. *45*, e51.

Mou, H., Zhao, R., Sherwood, R., Ahfeldt, T., Lapey, A., Wain, J., Sicilian, L., Izvolsky, K., Lau, F.H., Musunuru, K., et al. (2012). Generation of multipotent lung and airway progenitors from mouse ESCs and patient-specific cystic fibrosis iPSCs. Cell Stem Cell *10*, 385–397.

Nikolic, M.Z., Caritg, O., Jeng, Q., Johnson, J.-A., Sun, D., Howell, K.J., Brady, J.L., Laresgoiti, U., Allen, G., Butler, R., et al. (2017). Human embryonic lung epithelial tips are multipotent progenitors that can be expanded in vitro as long-term self-renewing organoids. eLife *6*, e26575.

Ogawa, S., Surapisitchat, J., Virtanen, C., Ogawa, M., Niapour, M., Sugamori, K.S., Wang, S., Tamblyn, L., Guillemette, C., Hoffmann,

E., et al. (2013). Three-dimensional culture and cAMP signaling promote the maturation of human pluripotent stem cell-derived hepatocytes. Development *140*, 3285–3296.

Onieva, J., Ross, J., Harmouche, R., Yarmarkovich, A., Lee, J., Diaz, A., Washko, G.R., and Estépar, R.S. (2016). Chest imaging platform: an open-source library and workstation for quantitative chest imaging. Int. J. Comput. Assist. Radiol. Surg. *11*(Suppl. 1), S40–S41.

Park, S., Gianotti-Sommer, A., Molina-Estevez, F.J., Vanuytsel, K., Skvir, N., Leung, A., Rozelle, S.S., Shaikho, E.M., Weir, I., Jiang, Z., et al. (2017). A comprehensive, ethnically diverse library of sickle cell disease-specific induced pluripotent stem cells. Stem Cell Reports *8*, 1076–1085.

Pashos, E.E., Park, Y., Wang, X., Raghavan, A., Yang, W., Abbey, D., Peters, D.T., Arbelaez, J., Hernandez, M., Kuperwasser, N., et al. (2017). Large, diverse population cohorts of hiPSCs and derived hepatocyte-like cells reveal functional genetic variation at blood lipid-associated loci. Cell Stem Cell *20*, 558–570.

Rashid, S.T., Corbineau, S., Hannan, N., Marciniak, S.J., Miranda, E., Alexander, G., Huang-Doran, I., Griffin, J., Ahrlund-Richter, L., Skepper, J., et al. (2010). Modeling inherited metabolic disorders of the liver using human induced pluripotent stem cells. J. Clin. Invest. *120*, 3127–3136.

Reeves, E.P., O'Dwyer, C.A., Dunlea, D.M., Wormald, M.R., Hawkins, P., Alfares, M., Kotton, D.N., Rowe, S.M., Wilson, A.A., and McElvaney, N.G. (2018). Ataluren, a new therapeutic for alpha-1 antitrypsin-deficient individuals with nonsense mutations. Am. J. Respir. Crit. Care Med. *198*, 1099–1102.

Ross, J.C., Estépar, R.S., Diaz, A., Westin, C.-F., Kikinis, R., Silverman, E.K., and Washko, G.R. (2009). Lung extraction, lobe segmentation and hierarchical region assessment for quantitative analysis on high resolution computed tomography images. Med. Image. Comput. Comput. Assist. Interv. *12*, 690–698.

Segeritz, C.-P., Rashid, S.T., de Brito, M.C., Serra, M.P., Ordoñez, A., Morell, C.M., Kaserman, J.E., Madrigal, P., Hannan, N.R.F., Gatto, L., et al. (2018). hiPSC hepatocyte model demonstrates the role of unfolded protein response and inflammatory networks in α_1-antitrypsin deficiency. J. Hepatol. *69*, 851–860.

Somers, A., Jean, J.-C., Sommer, C.A., Omari, A., Ford, C.C., Mills, J.A., Ying, L., Sommer, A.G., Jean, J.M., Smith, B.W., et al. (2010). Generation of transgene-free lung disease-specific human induced pluripotent stem cells using a single excisable lentiviral stem cell cassette. Stem Cells *28*, 1728–1740.

Sommer, C.A., Stadtfeld, M., Murphy, G.J., Hochedlinger, K., Kotton, D.N., and Mostoslavsky, G. (2009). Induced pluripotent stem cell generation using a single lentiviral stem cell cassette. Stem Cells *27*, 543–549.

Smith, C., Abalde-Atristain, L., He, C., Brodsky, B.R., Braunstein, E.M., Chaudhari, P., Jang, Y.-Y., Cheng, L., and Ye, Z. (2015). Efficient and allele-specific genome editing of disease loci in human iPSCs. Mol. Ther. *23*, 570–577.

Tafaleng, E.N., Chakraborty, S., Han, B., Hale, P., Wu, W., Soto-Gutierrez, A., Feghali-Bostwick, C.A., Wilson, A.A., Kotton, D.N., Nagaya, M., et al. (2015). Induced pluripotent stem cells model personalized variations in liver disease resulting from α_1-antitrypsin deficiency. Hepatology *62*, 147–157.

Tan, L., Dickens, J.A., Demeo, D.L., Miranda, E., Perez, J., Rashid, S.T., Day, J., Ordonez, A., Marciniak, S.J., Haq, I., et al. (2014). Circulating polymers in α_1-antitrypsin deficiency. Eur. Respir. J. *43*, 1501–1504.

Warren, C.R., O'Sullivan, J.F., Friesen, M., Becker, C.E., Zhang, X., Liu, P., Wakagayashi, Y., Morningstar, J.E., Shi, X., Choi, J., et al. (2017). Induced pluripotent stem cell differentiation enables functional validation of GWAS variants in metabolic disease. Cell Stem Cell *20*, 547–557.

Wilson, A.A., Ying, L., Liesa, M., Segeritz, C.-P., Mills, J.A., Shen, S.S., Jean, J., Lonza, G.C., Liberti, D.C., Lang, A.H., et al. (2015). Emergence of a stage-dependent human liver disease signature with directed differentiation of alpha-1 antitrypsin-deficient iPS cells. Stem Cell Reports *4*, 873–885.

Yusa, K., Rashid, S.T., Strick-Marchand, H., Varela, I., Liu, P.-Q., Paschon, D.E., Miranda, E., Ordonez, A., Hannan, N.R.F., Rouhani, F.J., et al. (2012). Targeted gene correction of α_1-antitrypsin deficiency in induced pluripotent stem cells. Nature *478*, 391–394.